Heterogeneous expression of the SARS-Coronavirus-2 receptor ACE2 in the human respiratory tract

Miguel E. Ortiz Bezara[1], Andrew Thurman[2], Alejandro A. Pezzulo[2], Mariah R. Leidinger[3], Julia A. Klesney-Tait[2], Philip H. Karp[2], Ping Tan[2], Christine Wohlford-Lenane[1], Paul B. McCray, Jr.[1*], David K. Meyerholz[3*]

Departments of Pediatrics[1], Internal Medicine[2], and Pathology[3]; University of Iowa College of Medicine, University of Iowa, Iowa City, IA USA

*Contributed equally

Correspondence:

David K. Meyerholz (david-meyerholz@uiowa.edu)

Paul B. McCray, Jr. (paul-mccray@uiowa.edu)

Running title: Expression of ACE2 in the human respiratory tract

Competing interest declaration:

The authors declare no competing interests.

Abstract:

Zoonotically transmitted coronaviruses are responsible for three disease outbreaks since 2002, including the current COVID-19 pandemic, caused by SARS-CoV-2. Its efficient transmission and range of disease severity raise questions regarding the contributions of virus-receptor interactions. ACE2 is a host ectopeptidase and the receptor for SARS-CoV-2. Despite numerous reports describing ACE2 mRNA abundance and tissue distribution, there remains a paucity of data evaluating ACE2 protein and its correlation with other SARS-CoV-2 susceptibility factors. Here, we systematically examined the human upper and lower respiratory tract using single-cell RNA sequencing and immunohistochemistry to determine receptor expression and evaluated its association with risk factors for severe COVID-19. Our results reveal that ACE2 protein is highest within the sinonasal cavity and pulmonary alveoli, sites of presumptive viral transmission and severe disease development, respectively. In the lung parenchyma, ACE2 protein was found on the apical surface of a small subset of alveolar type II cells and colocalized with TMPRSS2, a cofactor for SARS-CoV2 entry. ACE2 protein was not increased by pulmonary risk factors for severe COVID-19. However, ACE2 protein was increased in children, a demographic with a reduced incidence of severe COVID-19. These results offer new insights into ACE2 localization and function in susceptibility to COVID-19.

Key words: Lung, expression, alveolar type II cells, ciliated cells, immunohistochemistry

Introduction:

Angiotensin-converting enzyme 2 (ACE2) is the cellular receptor for both severe acute respiratory syndrome coronavirus (SARS-CoV) and SARS-CoV-2 (1, 2). SARS-CoV caused a pneumonia outbreak in 2002-2003 with a mortality rate of 9.6% and over 800 deaths worldwide (3). SARS-CoV-2 is the etiologic agent of coronavirus disease 2019 (COVID-19) which was first recognized in December 2019 and has now reached pandemic proportions (2, 4). SARS-CoV-2 infection can be fatal, with the risk for increased disease severity correlating with advanced age and underlying comorbidities, while children and younger individuals generally have milder disease (5-8). These trends in disease severity could reflect differences in ACE2 distribution and expression in the respiratory tract.

Previous studies have evaluated ACE2 expression in the respiratory tract. Studies of ACE2 mRNA transcript abundance have provided conflicting interpretations, as well as a lack of protein validation (9-16). ACE2 protein studies have been limited by a paucity of lung tissue substrates and reports that have yielded contradictory results (17-20) (Supplemental Table 1). It is reported that some clinical factors (sex, age, or presence of comorbidities) could influence ACE2 expression in the human lower respiratory tract. The ACE2 gene resides on the X chromosome and therefore could be differentially regulated between males and females due to variable X-inactivation (21). Increased abundance of circulating ACE2 protein is reported to correlate with male sex, advanced age, and chronic comorbidities such as diabetes, cardiovascular disease, and renal disease (reviewed in (22)). Recent single-cell mRNA sequencing (scRNA-seq) studies of respiratory tract cells have reported contradictory evidence regarding the correlation between ACE2 transcript abundance and age, sex, smoking status, and other comorbidities (9-14).

We investigated the hypothesis that ACE2 drives disease severity in susceptible patient populations through enhanced abundance or distribution in different locations or cell types of the respiratory tract. We reanalyzed publicly available scRNA-seq data from distal lung biopsies (23), nasal brushings and nasal turbinate samples (24) to evaluate ACE2 transcript abundance in specific cell types. We complemented these analyses with optimized and validated ACE2 immunostaining protocols, to corroborate single cell analyses as well as to screen for differences in cellular ACE2 protein in lung tissues derived from a cohort of control and chronic diseased patients.

Results:

In the alveoli, ACE2 transcripts were detected mostly in alveolar type II (AT2) cells (89.5% of all $ACE2^+$ cells) (Figure 1a), but specifically within a subset of these cells (1.2% of AT2 cells) (Figure 1b, Supplemental Figure 1a-b). These data indicate ACE2 transcripts are uncommon in most alveolar cell types. Alveoli had apical ACE2 protein only in a small number (usually ~1% or less) of AT2 cells (Figure 1c), consistent with the scRNA-seq results. The identity of these cells was confirmed by co-staining for surfactant protein-C. These $ACE2^+$ AT2 cells were observed within areas of alveolar collapse (Figures 1d-f) and had morphologic features of hyperplastic AT2 cells, being more plump and larger than $ACE2^-$ AT2 cells in the same tissue section (Figure 1g). Interestingly, alveolar macrophages were negative for ACE2 protein staining by immunohistochemistry, despite previous reports of ACE2 protein in these cells (Supplemental Table 1). The lack of ACE2 transcripts in macrophages was also confirmed by scRNA-seq data that revealed ACE2 mRNA in only 0.1% of macrophages, monocytes, or dendritic cells (Supplemental Figure 1a-b). The concordance between scRNA-seq and immunohistochemistry results provides compelling evidence that ACE2 is primarily present in a subset of AT2 cells and that alveolar macrophages lack ACE2.

Recent evidence indicates that proteases such as TMPRSS2 facilitate entry of SARS-CoV-2 into $ACE2^+$ cells (25). We evaluated scRNA-seq data and observed that TMPRSS2 mRNA was present in 35.5% of all AT2 cells (Figure 2a) but was more prevalent (50.0%) in $ACE2^+$ AT2 cells (Figure 2b). Additionally, we observed colocalization of ACE2 and TMPRSS2 on the apical membrane of these AT2 cells (Figure 2c). These findings suggest that AT2 cells

with apical ACE2 and TMPRSS2 could readily facilitate SARS-CoV-2 cellular infection and disease as seen in COVID-19 patients.

We next evaluated ACE2 in the conducting airways (trachea, bronchi, bronchioles). In the trachea and bronchi, apical ACE2 was rare and limited to ciliated cells (Figure 3a), similar to localization results in primary cultures of well-differentiated human airway epithelial cells (26). In the submucosal glands of large airways, occasional serous cells and vessels near the acini were positive for ACE2 (Supplemental Figures 2a-b). In bronchioles, ACE2 was regionally localized (Figures 3b-d). These findings show nominal detection of ACE2, corresponding with the lack of primary airway disease (e.g., bronchitis, etc.) seen in COVID-19 patients.

Detection of ACE2 protein has been variably reported in several small studies (18, 20). In this larger study, we saw that the regional distribution of ACE2 protein varied between donors. In the surface epithelium of trachea and bronchi, we detected ACE2 in only 12% and 27% of donors, respectively (Figure 4a). In the distal areas of the lung, ACE2 detection was more common, with bronchiolar and alveolar protein detection in 36% and 59% of donors, respectively (Figure 4a). A similar pattern of variable alveolar ACE2 was seen for mRNA transcripts in the scRNA-seq data, where 50% of donors showed low abudance in AT2 cells, and the other 50% of donors showed high abundance in the same cell type (Figure 4b). These findings suggest that ACE2 expression can vary between different lung regions and between individuals. Importantly, this low level of cellular protein provided us with an opportunity to investigate the potential for various clinical factors to increase ACE2 expression.

Independent risk factors associated with severe COVID-19 include male sex, increased age, and presence of comorbidities (6, 7, 27, 28). To evaluate whether the spatial distribution and abundance of ACE2 protein in the lower respiratory tract differed by these risk factors, we scored tissues for ACE2 protein detection (Supplemental Table 2). In the cohort, neither age nor sex were associated with ACE2 protein detection (using the median age as cut-off) (Figures 4c-d). Since recent studies of COVID-19 infections suggested that young children have reduced disease severity when infected by SARS-CoV-2 (6, 8), we compared lung tissue samples from children <10 years of age to those from the remaining older subjects (19-71 years of age) and found that ACE2 protein detection was higher in this subset of young children (Figure 4e). To test whether ACE2 distribution was affected by the presence of underlying diseases, we assessed the ACE2 localization pattern using tissues from subjects with chronic comorbidities (asthma, cardiovascular disease, chronic obstructive pulmonary disease, cystic fibrosis, diabetes, and smoking) and compared them to controls (Supplemental Table 2). The control group was similar in age to the chronic disease group (Figure 4f). We observed no significant differences between the two groups in ACE2 distribution, except for bronchioles, where ACE2 protein was reduced in the chronic disease group (Figure 4g, Supplemental Figure 2c). These results show that ACE2 levels in the respiratory tract were not increased in association with risk factors for severe COVID-19, such as male sex, advanced age, and underlying chronic comorbidities. Instead, we saw increased ACE2 detection in children <10 years of age and in the small airways (bronchioles) of individuals without chronic comorbidities in our cohort.

Given the unexpected heterogeneity in the lower respiratory tract, we also investigated ACE2 in the upper respiratory tract. scRNA-seq data from nasal brushing and nasal turbinate

samples (24) show ACE2 mRNA transcripts in 2-6% of epithelial cells (Supplemental Figure 3a-d). We then studied nasal biopsy tissues and found that ACE2 protein was detected in all tissue samples and, when present, was seen exclusively on the apical surface of ciliated cells. Distribution varied regionally based on the characteristics of the epithelium, with rare detection in thicker ciliated pseudostratified epithelium, and more abundant protein in thinner epithelium (Figures 5a-g). Thinner epithelial height is expected in specific regions including the floor of the nasal cavity, meatuses, and paranasal sinuses (29). The sinonasal cavity is an interface between the respiratory tract and the environment, and high SARS-CoV-2 viral loads can be detected in nasal swabs from infected patients (30), consistent with our ACE2 expression data. This reservoir of $ACE2^{+}$ cells may facilitate the reported transmission from individuals who have very mild or asymptomatic disease (31).

Discussion:

A critical aspect of this study was to evaluate ACE2 protein expression and distribution by immunohistochemistry to more accurately corroborate single cell transcript studies and better evaluate clinical groups for COVID-19 disease susceptibility. Previously, limited reports have variably shown ACE2 protein in the upper and lower respiratory tract, but cellular localization and distribution in human lung tissues have been inconsistent and contradictory (17-20) (Supplemental Table 1). *In vitro* studies demonstrate that ACE2 protein is found at the apical membrane of polarized airway epithelia, where it permits virus binding and cell entry (18, 26). In our study, ACE2 was consistently localized to the apical membranes of cells. ACE2 was more commonly found in the sinonasal cavity where transmission likely occurs and on AT2 cells of the lung parenchyma where severe disease develops. Expression of ACE2 in the sinonasal cavity could explain the high transmissibility of SARS-CoV-2 and HCoV-NL63, a cold-related coronavirus, which also uses ACE2 as a receptor. One mystery is why SARS-CoV, which also uses ACE2, was apprently less efficient at human-to-human transmission (32). Whether this represents differences in the interactions of SARS-CoV and SARS-CoV-2 with co-receptors (33) or other factors in the nasal cavity remains to be investigated.

SARS-CoV and SARS-CoV-2 both replicate in the lungs (34, 35), consistent with the ACE2 protein distribution defined in this study and suggested by previous studies (17, 18). We show that ACE2 and TMPRSS2 coexpress in AT2 cells at the mRNA and protein levels, suggesting susceptibility to infection. Additionally, it may also be possible that $TMPRSS2^{-}$ $ACE2^{+}$ AT2 cells can become infected through the use of other airway proteases (36). AT2 cells are critical for surfactant protein production and serve as progenitor cells for the AT1 cells, thus

damage to these AT2 cells could contribute to acute lung injury (37), which is a common feature of severe COVID-19 (5). Additionally, the larger morphology of $ACE2^+$ AT2 cells is consistent with a type of hyperplastic AT2 population that, if damaged, could affect the repair mechanisms of the alveoli. Infection of AT2 cells could disrupt epithelial integrity leading to alveolar edema, and facilitate viral spread to $ACE2^+$ interstitial cells/vessels for systemic virus dissemination, given that SARS-CoV-2 has been detected in pulmonary endothelium (38) and blood (39). Furthermore, cell-to-cell spread of coronaviruses to other epithelial cells after initial infection could also occur via receptor-independent mechanisms related to the fusogenic properties of the S protein (40). It is interesting that computerized tomography studies of early disease in people with COVID-19 demonstrate patchy ground glass opacities in the peripheral and posterior lungs, regions that are more susceptible to alveolar collapse (41).

ACE2 protein detection in the lower respiratory tract was heterogeneous. The relatively small number of $ACE2^+$ cells found in our study proved advantageous in evaluating whether conditions that predispose to severe disease also increased cellular ACE2 expression, but this was not observed. Rather we saw elevated ACE2 protein in demographic pools with expected low risk for severe COVID-19 (young children and in bronchioles of the control group) and these results suggest alternative explanations. First, the potential relationship between ACE2 abundance in the respiratory tract and severe COVID-19 is likely complex. On one hand, more receptor availability could enhance viral entry into cells and worsen disease outcomes; alternatively, ACE2 may play a protective role in acute lung injury through its enzymatic activity (42-44) and therefore could improve disease outcomes. Our data would support the latter and implicate a dualistic role for ACE2 as both a viral receptor and a protective agent in acute lung

injury. Additionally, ACE2 exists in cell-associated and soluble forms (45). It is possible that greater ACE2 expression could result in increased soluble ACE2 in respiratory secretions where it might act as a decoy receptor and reduce virus entry (1, 46). Second, other factors such as TMPRSS2 expression might be more important in regulating disease severity. TMPRSS2 on the apical membrane of AT2 cells might facilitate SARS-CoV-2 entry when ACE2 is rare or even below the limit of detection in this study. Third, low levels of the receptor could be sufficient for the virus to infect and cause severe disease. Importantly, unlike SARS or HCoV-NL63, the SARS-CoV-2 spike glycoproteins undergo proteolytic processing at a multibasic S1/S2 site by furin intracellularly, prior to virion release (25, 47). Additionally, compared to SARS-CoV, the SARS-CoV-2 receptor binding motif has a higher affinity for ACE2 (48, 49). These features may enhance the ability of SARS-CoV-2 to bind to cells, undergo S2' cleavage by TMPRSS2 or other surface proteases, fuse to the host cell membrane, and release its genome. It is important to mention that the lack of correlation between SARS-CoV-2 receptor expression and disease severity contrasts with another severe coronavirus disease, MERS, where comorbidities were observed to increase its receptor detection in respiratory tissues (50, 51).

mRNA transcript abundance is not always representative of protein levels (52), and therefore both should be evaluated in conjunction before making conclusions about gene expression. Some of the factors that account for these differences include post-transcriptional regulation or rapid protein turnover. Additionally, other factors limit direct comparisons between scRNA-seq results and protein staining, including sample size, tissue heterogeneity, and undefined biopsy sites. In the alveoli, we show ACE2 protein in a small subset of AT2 cells, which correlates with the scRNA-seq data and with other RNA sequencing publications (11, 15,

16). In the lower airways and sinonasal cavity, RNA sequencing data indicate ACE2 transcripts in both ciliated and secretory cells (11, 15, 16), but we show ACE2 protein is only found in ciliated cells. Likewise, some authors have reported lower ACE2 transcript abundance in children (9, 12) and suggested this finding as an explanation for the lower disease severity in this age group. In contrast, we show that children have more cellular ACE2 protein than older adults, and while children are likely at similar risk for infection (8, 53) they appear protected from severe lung disease, possibly through enhanced ACE2 protein.

In summary, we find that ACE2 protein has heterogeneous expression in the respiratory tract with more frequent ACE2 detection in the sinonasal epithelium and AT2 cells that correlates with putative sites for transmission and severe disease, respectively. The small subset of $ACE2^{+}$ AT2 cells in the lung could be further studied to reveal factors regulating ACE2 expression and clarify potential targets for antiviral therapies. Contrary to our initial hypothesis, we saw no increase of ACE2 protein in the chronic disease group. Interestingly, we observed increased ACE2 in young children and control group bronchioles, suggesting a possible protective effect by ACE2 expression. These results suggest that features driving disease susceptibility and severity are complex. Factors other than ACE2 protein abundance, including viral load, host innate and adaptive immune responses, and the activities of the pulmonary renin-angiotensin system may also be important determinants of outcomes.

Materials and methods:

Tissues:

Studies on human tissues were approved by the institutional review board of the University of Iowa. Tissues included nasal biopsies (n=3, deidentified and lacked evidence of significant disease or cancer), lung donors, primary cell cultures (54), and autopsy tissues (control tissues) that were selected from archival repositories as formalin-fixed paraffin-embedded blocks. Lung cases were selected to comprise two case study groups: 1) Chronic disease group was defined as having chronic comorbidities including: asthma, cardiovascular disease, chronic obstructive pulmonary disease, cystic fibrosis, diabetes, and smoking. 2) Control group was defined as lacking these chronic comorbidities and lacking clinical lung disease. The definition of chronic comorbidities was informed by reported independent risk factors for mortality in COVID-19 (7).The cumulative cohort included 29 cases (15 chronic comorbidities and 14 controls) with a broad range of ages (0.5 – 71 years) and both sexes were represented (13 female and 16 male). For these lungs, if a trachea or bronchus tissue block was available from the same case – these were included as well (Supplemental Table 2). Bronchioles were observed in most lung sections and were defined as intrapulmonary airways lacking evidence of cartilage or submucosal glands (55).

Immunohistochemistry and immunofluorescence:

All formalin-fixed paraffin-embedded tissues were sectioned (~4 µm) and hydrated through a series of xylene and alcohol baths to water. Immunohistochemical techniques were used for the following markers: angiotensin-converting enzyme 2 (ACE2) (26), allograft inflammatory factor

1 (AIF1, also known as IBA1) (56), surfactant protein C (SP-C) (57), and mucin 5B (MUC5B) (56). For more specifics about the reagents please see Supplemental Table 3.

The immunostaining protocols for ACE2 were rigorously optimized and validated to avoid nonspecific staining that is commonplace and give confidence in the sensitivity of the protocol and quality of the tissues (Supplemental Figure 4, Supplemental Table 1 and Supplemental Table 3). We analyzed ACE2 protein expression in human upper and lower respiratory tract by immunohistochemistry (Supplemental Table 2). Human respiratory tract tissues were scored for ACE2 expression by a masked pathologist, following principles for reproducible tissue scores (17).

For immunofluorescence, formalin-fixed and paraffin-embedded human lung blocks were sectioned (~4 µm). Slides were baked (55°C x 15 min) and then deparaffinized (hydrated) in a series of xylene and progressive alcohol baths. Antigen retrieval was performed using Antigen Unmasking Solution (1:100, #H-3300) in citrate buffer (pH 6.0) solution to induce epitope retrieval (5 min x 3 times) in the microwave. Slides were washed (PBS, 3 times, 5 min each) and a PAP pen used to encircle the tissue. Slides were blocked with background blocking solution (2% BSA in Superblock 1 hr in humid chamber). Primary antibodies anti-ACE2 (1:100, Mouse monoclonal, MAB933, R&D Systems, Minneapolis, MN USA) and anti-TMPRSS2 (1:200, Rabbit monoclonal, #ab92323, Abcam, Cambridge, MA USA) were diluted in blocking solution (2% BSA in Superblock overnight 4°C). Secondary antibodies anti-mouse Alexa568 (for ACE2) and anti-rabbit Alexa488 (for TMPRSS2) were applied at a concentration of 1:600 for 1 hour at room temperature. Slides were washed and mounted with Vectashield containing DAPI.

Tissue scoring:

Stained tissue sections were examined for ACE2 localization using a post-examination method for masking and scored by a masked pathologist following principles for reproducible tissue scores (58). The initial examination showed a low heterogenous incidence of ACE2 staining for various tissues, so the following ordinal scoring system was employed to quantify number of staining-positive cells: 0 = below the limit of detection; 1 = <1%; 2 = 1-33%; 3 = 34-66%; and 4 = >66% of cells. For these anatomic regions (e.g. airway or alveoli), cell counts for each tissue were made to know the population density per microscopic field to make reproducible interpretations. For determination of AT2 cell size, ACE2 and SP-C protein immunostaining were evaluated on the same lung tissue section for each case. A region of minimally diseased lung was examined and SP-C$^+$ AT2 cells were measured for diameter in the plane perpendicular to the basement membrane. Similar measurements were then made for ACE2$^+$/SP-C$^+$ cells.

Analysis of single cell RNA sequencing data:

Single cell RNA sequencing data sets were accessed from Gene Expression Omnibus (GEO) series GSE121600 (24) and GSE122960 (23). For GSE121600, raw H5 files for bronchial biopsy (GSM3439925), nasal brushing (GSM3439926), and turbinate (GSM3439927) samples were downloaded, and barcodes with less than 1000 unique molecular identifiers (UMIs) were discarded. For GSE122960, filtered H5 files for eight lung transplant donor samples from lung parenchyma (GSM3489182, GSM3489185, GSM3489187, GSM3489189, GSM3489191, GSM3489193, GSM3489195, GSM3489197) were downloaded, and all barcodes were retained. The eight donors varied from 21-63 years of age (median age = 48) and were composed of five

306 African American, one Asian, and two white donors, and 2 active, 1 former, and 5 never
307 smokers. Gene count matrices from the eight donors were aggregated for analysis.
308
309 For the bronchial biopsy sample, 82.4% of cells had less than 3,000 UMIs, so we lacked
310 confidence in assigned cell types, and thus results were not reported. The other three data sets
311 (nasal brushing, turbinate, and lung parenchyma) were processed in a similar manner. Gene-by-
312 barcode count matrices were normalized, log-transformed, and scaled followed by dimension
313 reduction using principal components analysis (PCA). Principal components were used to obtain
314 uniform manifold approximation and projection (UMAP) visualizations, and cells were clustered
315 using a shared nearest neighbor (SNN) approach with resolution parameter 0.4, giving 14
316 clusters for nasal brushing, 15 clusters for turbinate, and 28 clusters for lung parenchyma. Cell
317 types associated with each cluster were identified by determining marker genes for each cluster
318 and comparing the list of marker genes to known cell type markers (Supplemental Figure 5). All
319 analyses were performed using R package Seurat version 3.1.1 (59). In the nasal brushing
320 sample, we were unable to associate a cell type with one cluster containing 776 cells (16.5%) due
321 to low UMIs, so these cells were discarded.
322
323 For the lung parenchyma data, gene expression in alveolar type II cells for a single donor was
324 quantified by summing up gene counts for all alveolar type II cells and dividing by total UMIs
325 for all alveolar type II cells to get normalized counts, followed by rescaling the normalized
326 counts to obtain counts per million (CPM).
327
328 **Statistical analyses:**

Statistical analyses for group comparisons and tissue scoring data were performed using GraphPad Prism version 8 (GraphPad Software, La Jolla, CA USA). Mann Whitney U tests or T-tests were used for group comparisons as appropriate. ACE2 protein detection in different tissues was analyzed using the ordinal scoring system (0-4) and Cochran-Armitage test for trend.

334 **Author contributions:**

335 Conceptualization and writing – original draft, M.O.B., P.B.M. and D.K.M.; Data curation, A.T.;
336 Formal analysis, M.O.B., A.T., A.P. and D.K.M.; Investigation, A.T., A.P., M.R.L., C.W.-L. and
337 D.K.M.; Visualization, M.O.B., A.T., D.K.M.; Resources, A.P., J.A.K.-T., P.H.K., P.T., P.B.M.
338 and D.K.M.; Writing – review and editing, M.O.B, A.T., A.P., M.R.L., J.A.K.-T., P.H.K., P.T.,
339 C.W.-L., P.B.M. and D.K.M

340

341 **Acknowledgements:**

342 We thank our laboratory members and colleagues Stanley Perlman, Robert Robinson, and
343 Thomas Gallagher for their helpful discussion and technical assistance.

344

345 This work is supported by the National Institutes of Health (NIH) Grant P01 AI060699; and the
346 Pathology Core, which are partially supported by the Center for Gene Therapy for Cystic
347 Fibrosis (NIH Grant P30 DK-54759), and the Cystic Fibrosis Foundation. P.B.M. is supported by
348 the Roy J. Carver Charitable Trust.

References:

1. Li W, Moore MJ, Vasilieva N, Sui J, Wong SK, Berne MA, et al. Angiotensin-converting enzyme 2 is a functional receptor for the SARS coronavirus. *Nature.* 2003;426(6965):450-4.
2. Zhou P, Yang XL, Wang XG, Hu B, Zhang L, Zhang W, et al. A pneumonia outbreak associated with a new coronavirus of probable bat origin. *Nature.* 2020.
3. Lam CW, Chan MH, and Wong CK. Severe acute respiratory syndrome: clinical and laboratory manifestations. *Clin Biochem Rev.* 2004;25(2):121-32.
4. Wilder-Smith A, Chiew CJ, and Lee VJ. Can we contain the COVID-19 outbreak with the same measures as for SARS? *Lancet Infect Dis.* 2020.
5. Zhou F, Yu T, Du R, Fan G, Liu Y, Liu Z, et al. Clinical course and risk factors for mortality of adult inpatients with COVID-19 in Wuhan, China: a retrospective cohort study. *Lancet.* 2020.
6. Guan WJ, Ni ZY, Hu Y, Liang WH, Ou CQ, He JX, et al. Clinical Characteristics of Coronavirus Disease 2019 in China. *N Engl J Med.* 2020.
7. Mehra MR, Desai SS, Ruschitzka F, and Patel AN. Hydroxychloroquine or chloroquine with or without a macrolide for treatment of COVID-19: a multinational registry analysis. *The Lancet.* 2020.
8. Dong Y, Mo X, Hu Y, Qi X, Jiang F, Jiang Z, et al. Epidemiology of COVID-19 Among Children in China. *Pediatrics.* 2020.
9. Bunyavanich S, Do A, and Vicencio A. Nasal Gene Expression of Angiotensin-Converting Enzyme 2 in Children and Adults. *JAMA.* 2020.
10. Li G, He X, Zhang L, Ran Q, Wang J, Xiong A, et al. Assessing ACE2 expression patterns in lung tissues in the pathogenesis of COVID-19. *J Autoimmun.* 2020:102463.
11. Lukassen S, Chua RL, Trefzer T, Kahn NC, Schneider MA, Muley T, et al. SARS-CoV-2 receptor ACE2 and TMPRSS2 are primarily expressed in bronchial transient secretory cells. *EMBO J.* 2020;39(10):e105114.
12. Muus C, Luecken MD, Eraslan G, Waghray A, Heimberg G, Sikkema L, et al. Integrated analyses of single-cell atlases reveal age, gender, and smoking status associations with cell type-specific expression of mediators of SARS-CoV-2 viral entry and highlights inflammatory programs in putative target cells. *bioRxiv.* 2020.
13. Pinto BG, Oliveira AE, Singh Y, Jimenez L, Goncalves AN, Ogava RL, et al. ACE2 Expression is Increased in the Lungs of Patients with Comorbidities Associated with Severe COVID-19. *medRxiv.* 2020.
14. Smith JC, Sausville EL, Girish V, Yuan ML, Vasudevan A, John KM, et al. Cigarette smoke exposure and inflammatory signaling increase the expression of the SARS-CoV-2 receptor ACE2 in the respiratory tract. *Dev Cell.* 2020.
15. Sungnak W, Huang N, Becavin C, Berg M, Queen R, Litvinukova M, et al. SARS-CoV-2 entry factors are highly expressed in nasal epithelial cells together with innate immune genes. *Nat Med.* 2020;26(5):681-7.
16. Ziegler CGK, Allon SJ, Nyquist SK, Mbano IM, Miao VN, Tzouanas CN, et al. SARS-CoV-2 Receptor ACE2 Is an Interferon-Stimulated Gene in Human Airway Epithelial Cells and Is Detected in Specific Cell Subsets across Tissues. *Cell.* 2020.
17. Hamming I, Timens W, Bulthuis ML, Lely AT, Navis G, and van Goor H. Tissue distribution of ACE2 protein, the functional receptor for SARS coronavirus. A first step in understanding SARS pathogenesis. *J Pathol.* 2004;203(2):631-7.

18. Ren X, Glende J, Al-Falah M, de Vries V, Schwegmann-Wessels C, Qu X, et al. Analysis of ACE2 in polarized epithelial cells: surface expression and function as receptor for severe acute respiratory syndrome-associated coronavirus. *J Gen Virol.* 2006;87(Pt 6):1691-5.
19. Bertram S, Glowacka I, Muller MA, Lavender H, Gnirss K, Nehlmeier I, et al. Cleavage and activation of the severe acute respiratory syndrome coronavirus spike protein by human airway trypsin-like protease. *J Virol.* 2011;85(24):13363-72.
20. Bertram S, Heurich A, Lavender H, Gierer S, Danisch S, Perin P, et al. Influenza and SARS-coronavirus activating proteases TMPRSS2 and HAT are expressed at multiple sites in human respiratory and gastrointestinal tracts. *PLoS One.* 2012;7(4):e35876.
21. Carrel L, and Willard HF. X-inactivation profile reveals extensive variability in X-linked gene expression in females. *Nature.* 2005;434(7031):400-4.
22. Anguiano L, Riera M, Pascual J, and Soler MJ. Circulating ACE2 in Cardiovascular and Kidney Diseases. *Curr Med Chem.* 2017;24(30):3231-41.
23. Reyfman PA, Walter JM, Joshi N, Anekalla KR, McQuattie-Pimentel AC, Chiu S, et al. Single-Cell Transcriptomic Analysis of Human Lung Provides Insights into the Pathobiology of Pulmonary Fibrosis. *Am J Respir Crit Care Med.* 2019;199(12):1517-36.
24. Ruiz Garcia S, Deprez M, Lebrigand K, Cavard A, Paquet A, Arguel MJ, et al. Novel dynamics of human mucociliary differentiation revealed by single-cell RNA sequencing of nasal epithelial cultures. *Development.* 2019;146(20).
25. Hoffmann M, Kleine-Weber H, Schroeder S, Kruger N, Herrler T, Erichsen S, et al. SARS-CoV-2 Cell Entry Depends on ACE2 and TMPRSS2 and Is Blocked by a Clinically Proven Protease Inhibitor. *Cell.* 2020.
26. Jia HP, Look DC, Shi L, Hickey M, Pewe L, Netland J, et al. ACE2 receptor expression and severe acute respiratory syndrome coronavirus infection depend on differentiation of human airway epithelia. *J Virol.* 2005;79(23):14614-21.
27. Lu Q, and Shi Y. Coronavirus disease (COVID-19) and neonate: What neonatologist need to know. *J Med Virol.* 2020.
28. Mo P, Xing Y, Xiao Y, Deng L, Zhao Q, Wang H, et al. Clinical characteristics of refractory COVID-19 pneumonia in Wuhan, China. *Clin Infect Dis.* 2020.
29. Sternberg SS. *Histology for Pathologists.* Philadelphia, PA USA: Lippincott-Raven Publishers; 1997.
30. Wang W, Xu Y, Gao R, Lu R, Han K, Wu G, et al. Detection of SARS-CoV-2 in Different Types of Clinical Specimens. *JAMA.* 2020.
31. Bai Y, Yao L, Wei T, Tian F, Jin DY, Chen L, et al. Presumed Asymptomatic Carrier Transmission of COVID-19. *JAMA.* 2020.
32. Wang Y, Wang Y, Chen Y, and Qin Q. Unique epidemiological and clinical features of the emerging 2019 novel coronavirus pneumonia (COVID-19) implicate special control measures. *J Med Virol.* 2020.
33. Wrapp D, Wang N, Corbett KS, Goldsmith JA, Hsieh CL, Abiona O, et al. Cryo-EM structure of the 2019-nCoV spike in the prefusion conformation. *Science.* 2020;367(6483):1260-3.
34. Yen YT, Liao F, Hsiao CH, Kao CL, Chen YC, and Wu-Hsieh BA. Modeling the early events of severe acute respiratory syndrome coronavirus infection in vitro. *J Virol.* 2006;80(6):2684-93.
35. Zhang H, Zhou P, Wei Y, Yue H, Wang Y, Hu M, et al. Histopathologic Changes and SARS-CoV-2 Immunostaining in the Lung of a Patient With COVID-19. *Ann Intern Med.* 2020.
36. Ou X, Liu Y, Lei X, Li P, Mi D, Ren L, et al. Characterization of spike glycoprotein of SARS-CoV-2 on virus entry and its immune cross-reactivity with SARS-CoV. *Nat Commun.* 2020;11(1):1620.

37. Ware LB, and Matthay MA. The acute respiratory distress syndrome. *N Engl J Med.* 2000;342(18):1334-49.
38. Ackermann M, Verleden SE, Kuehnel M, Haverich A, Welte T, Laenger F, et al. Pulmonary Vascular Endothelialitis, Thrombosis, and Angiogenesis in Covid-19. *N Engl J Med.* 2020.
39. Chen W, Lan Y, Yuan X, Deng X, Li Y, Cai X, et al. Detectable 2019-nCoV viral RNA in blood is a strong indicator for the further clinical severity. *Emerg Microbes Infect.* 2020;9(1):469-73.
40. Gallagher TM, Buchmeier MJ, and Perlman S. Dissemination of MHV4 (strain JHM) infection does not require specific coronavirus receptors. *Adv Exp Med Biol.* 1993;342:279-84.
41. Song F, Shi N, Shan F, Zhang Z, Shen J, Lu H, et al. Emerging 2019 Novel Coronavirus (2019-nCoV) Pneumonia. *Radiology.* 2020;295(1):210-7.
42. Gu H, Xie Z, Li T, Zhang S, Lai C, Zhu P, et al. Angiotensin-converting enzyme 2 inhibits lung injury induced by respiratory syncytial virus. *Sci Rep.* 2016;6:19840.
43. Imai Y, Kuba K, Rao S, Huan Y, Guo F, Guan B, et al. Angiotensin-converting enzyme 2 protects from severe acute lung failure. *Nature.* 2005;436(7047):112-6.
44. Zou Z, Yan Y, Shu Y, Gao R, Sun Y, Li X, et al. Angiotensin-converting enzyme 2 protects from lethal avian influenza A H5N1 infections. *Nat Commun.* 2014;5:3594.
45. Lambert DW, Yarski M, Warner FJ, Thornhill P, Parkin ET, Smith AI, et al. Tumor necrosis factor-alpha convertase (ADAM17) mediates regulated ectodomain shedding of the severe-acute respiratory syndrome-coronavirus (SARS-CoV) receptor, angiotensin-converting enzyme-2 (ACE2). *J Biol Chem.* 2005;280(34):30113-9.
46. Hofmann H, Geier M, Marzi A, Krumbiegel M, Peipp M, Fey GH, et al. Susceptibility to SARS coronavirus S protein-driven infection correlates with expression of angiotensin converting enzyme 2 and infection can be blocked by soluble receptor. *Biochem Biophys Res Commun.* 2004;319(4):1216-21.
47. Hoffmann M, Kleine-Weber H, and Pohlmann S. A Multibasic Cleavage Site in the Spike Protein of SARS-CoV-2 Is Essential for Infection of Human Lung Cells. *Mol Cell.* 2020;78(4):779-84 e5.
48. Shang J, Ye G, Shi K, Wan Y, Luo C, Aihara H, et al. Structural basis of receptor recognition by SARS-CoV-2. *Nature.* 2020;581(7807):221-4.
49. Wan Y, Shang J, Graham R, Baric RS, and Li F. Receptor Recognition by the Novel Coronavirus from Wuhan: an Analysis Based on Decade-Long Structural Studies of SARS Coronavirus. *J Virol.* 2020;94(7).
50. Meyerholz DK, Lambertz AM, and McCray PB, Jr. Dipeptidyl Peptidase 4 Distribution in the Human Respiratory Tract: Implications for the Middle East Respiratory Syndrome. *Am J Pathol.* 2016;186(1):78-86.
51. Seys LJM, Widagdo W, Verhamme FM, Kleinjan A, Janssens W, Joos GF, et al. DPP4, the Middle East Respiratory Syndrome Coronavirus Receptor, is Upregulated in Lungs of Smokers and Chronic Obstructive Pulmonary Disease Patients. *Clin Infect Dis.* 2018;66(1):45-53.
52. Liu Y, Beyer A, and Aebersold R. On the Dependency of Cellular Protein Levels on mRNA Abundance. *Cell.* 2016;165(3):535-50.
53. Bi Q, Wu Y, Mei S, Ye C, Zou X, Zhang Z, et al. Epidemiology and transmission of COVID-19 in 391 cases and 1286 of their close contacts in Shenzhen, China: a retrospective cohort study. *Lancet Infect Dis.* 2020.
54. Itani OA, Chen JH, Karp PH, Ernst S, Keshavjee S, Parekh K, et al. Human cystic fibrosis airway epithelia have reduced Cl- conductance but not increased Na+ conductance. *Proc Natl Acad Sci U S A.* 2011;108(25):10260-5.
55. Meyerholz DK, Suarez CJ, Dintzis SM, and Frevert CW. *Comparative Anatomy and Histology: A Mouse, Rat and Human Atlas.* Academic Press - Elsevier; 2018.

56. Meyerholz DK, Lambertz AM, Reznikov LR, Ofori-Amanfo GK, Karp PH, McCray PB, Jr., et al. Immunohistochemical Detection of Markers for Translational Studies of Lung Disease in Pigs and Humans. *Toxicol Pathol.* 2016;44(3):434-41.
57. Krishnamurthy S, Wohlford-Lenane C, Kandimalla S, Sartre G, Meyerholz DK, Theberge V, et al. Engineered amphiphilic peptides enable delivery of proteins and CRISPR-associated nucleases to airway epithelia. *Nat Commun.* 2019;10(1):4906.
58. Meyerholz DK, and Beck AP. Principles and approaches for reproducible scoring of tissue stains in research. *Lab Invest.* 2018;98(7):844-55.
59. Stuart T, Butler A, Hoffman P, Hafemeister C, Papalexi E, Mauck WM, 3rd, et al. Comprehensive Integration of Single-Cell Data. *Cell.* 2019;177(7):1888-902 e21.

Figure 1

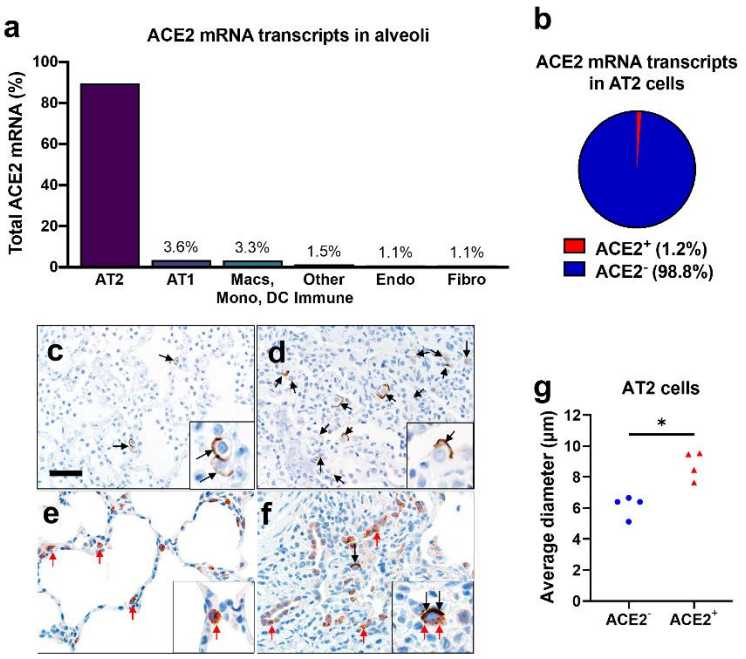

Figure 1. ACE2 expression in human lung. **a, b**) Single-cell RNA sequencing reanalysis of ACE2 transcript abundance in alveoli from lung parenchyma samples (23). Summative observations from all donors. Airway cells (basal, mitotic, ciliated, club) are not shown. **a**) 89.5% of the cells with detectable ACE2 mRNA in the alveoli are alveolar type II cells. **b**) Only 1.2% of alveolar type II cells have ACE2 mRNA transcripts. **c-f**) Detection of ACE2 protein (brown color, black arrows and insets) in representative sections of lower respiratory tract regions and tissue scoring (see Supplemental Table 2) (**g**). **c, d**) Alveolar regions had uncommon to regional polarized apical staining of solitary epithelial cells (**c**) that (when present) were more readily detected in collapsed regions of lung (**d**). **e, f**) SP-C (red arrows, inset) and ACE2 (black arrows, inset) dual immunohistochemistry on the same tissue sections. **e**) Non-collapsed regions had normal SP-C$^+$ AT2 cells lacking ACE2. **f**) Focal section of peri-airway remodeling and collapse with several SP-C$^+$ (red arrows) AT2 cells, but only a small subset of AT2 cells had prominent apical ACE2 protein (black arrows, inset). **g**) SP-C$^+$/ACE2$^+$ AT2 cells were often larger than SP-C$^+$/ACE2$^-$ AT2 cells from same lung sections (see also **d** and **e** insets) indicative of AT2 hypertrophy, each data point represents the average value for each case from 5-10 cell measurements per group, P=0.0014, paired T-test. AT2: alveolar type II. AT1: alveolar type I. Macs: Macrophages. Mono: Monocytes. DC: dendritic cells. Other immune cells: B cells, mast cells, natural killer/T cells. Endo: Endothelial. Fibro: Fibroblasts/myofibroblasts. Bar = 35 µm.

Figure 2

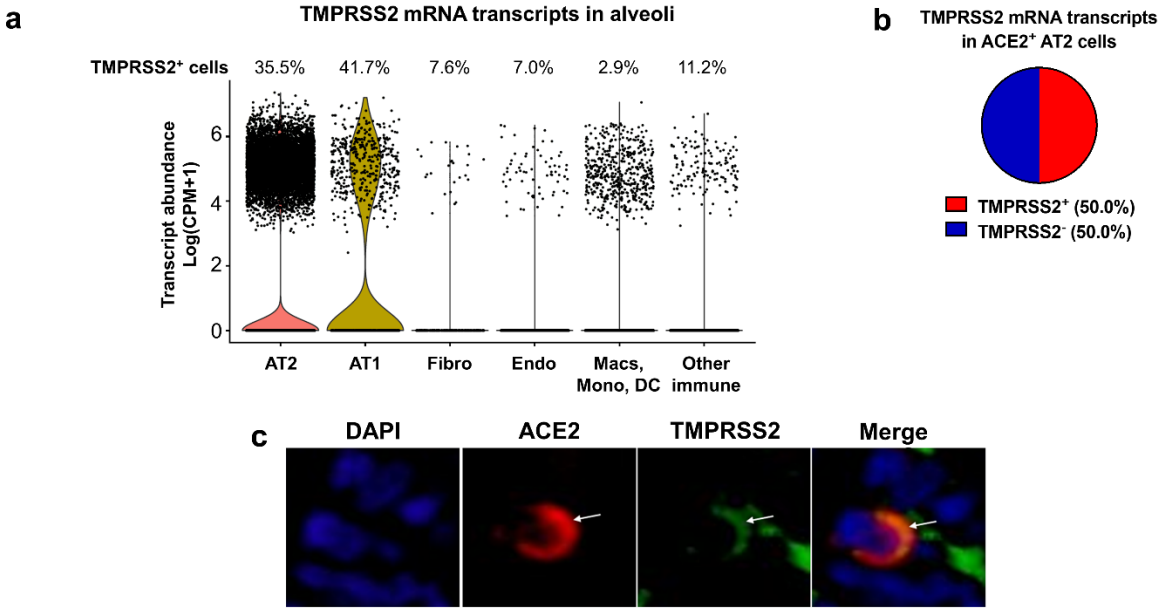

Figure 2. TMPRSS2 expression in the alveoli. **a, b**) Single-cell RNA sequencing reanalyses of TMPRSS2 transcript abundance in alveoli from lung parenchyma (23). Summative observations from all donors. **a**) Percentage of TMPRSS2$^+$ cells within each cell type shows TMPRSS2 transcripts in 35.5% of alveolar type II cells. Airway cells (basal, mitotic, ciliated, club) are not shown. Violin plots represent expression, each data point denotes a cell. **b**) TMPRSS2 transcripts in ACE2$^+$ alveolar type II cells. **c**) Immunofluorescence of alveoli shows apical colocalization of ACE2 and TMPRSS2 (white arrows). AT2: alveolar type II. AT1: alveolar type I. Macs: Macrophages. Mono: Monocytes. DC: dendritic cells. Other immune cells: B cells, mast cells, natural killer/T cells. Endo: Endothelial. Fibro: Fibroblasts/myofibroblasts. CPM: counts per million.

Figure 3

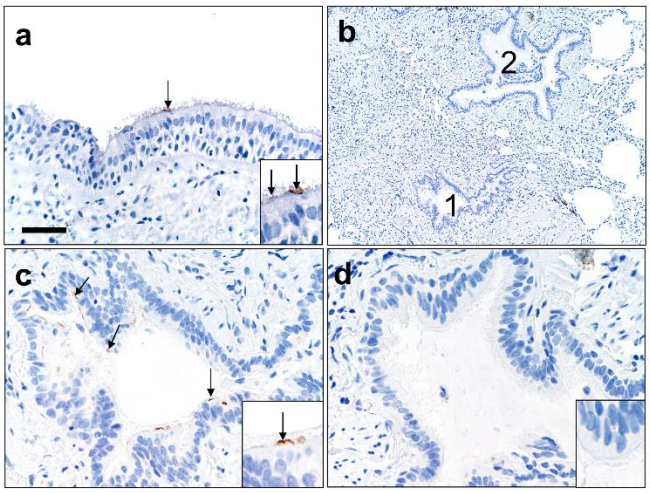

528

529 **Figure 3**. ACE2 protein in human lower airways. **a**) Large airways (trachea and bronchi)

530 exhibited rare ACE2 protein on the apical surface of ciliated cells. **b-d**) Small airways

531 (bronchioles) exhibited uncommon to localized apical ACE2 protein in ciliated cells (**c**, #1 in **b**)

532 while the adjacent bronchioles (**d**, #2 in **b**) lacked protein. Bar = 35 (a), 140 (b), and 70 μm (c,

533 d).

534

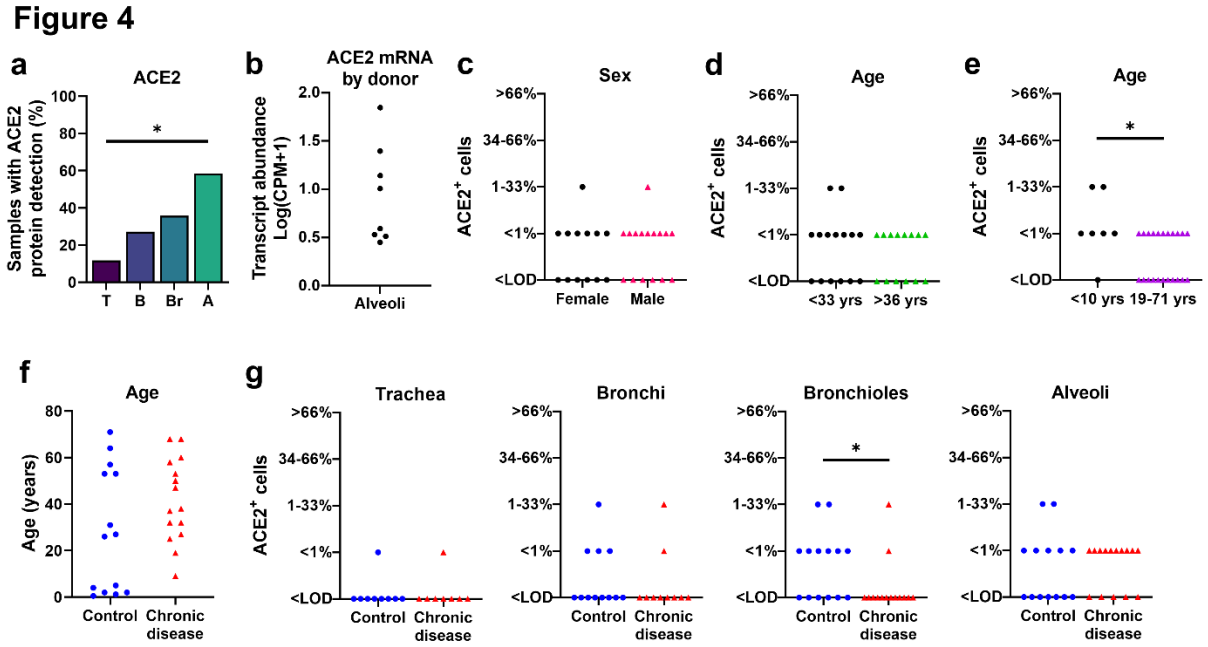

535

536 **Figure 4.** ACE2 distribution and scores in respiratory tissues. **a**) ACE2 protein had progressively
537 increased detection between donors in tissues from trachea (T), bronchi (B), bronchioles (Br), to
538 alveoli (A), (P=0.0009, Cochran-Armitage test for trend). **b**) Single-cell RNA sequencing
539 reanalyses of ACE2 mRNA transcript abundance in the alveoli shows variation between donors
540 (23). **c-d**) ACE2 protein scores from lung donors showed no differences based on sex or lower
541 vs. upper ages (using median age as a cut-off) (A, P=0.7338 and B, P=0.7053, Mann-Whitney U
542 test). **e**) ACE2 protein scores were elevated in young children (<10 yrs) compared to the
543 remaining subjects (19-71 yrs) (P=0.0282 Mann-Whitney U test). **f**) Control and chronic disease
544 groups did not have any significant differences in age (P=0.1362 Mann-Whitney U test). **g**)
545 ACE2 protein scores for trachea, bronchi, bronchiole, and alveoli in control versus chronic
546 disease groups (P= >0.9999, 0.6263, 0.0433, and 0.7359, respectively, Mann-Whitney U test).
547 Each symbol represents one donor. CPM: counts per million. LOD: Limit of detection.

548

Figure 5

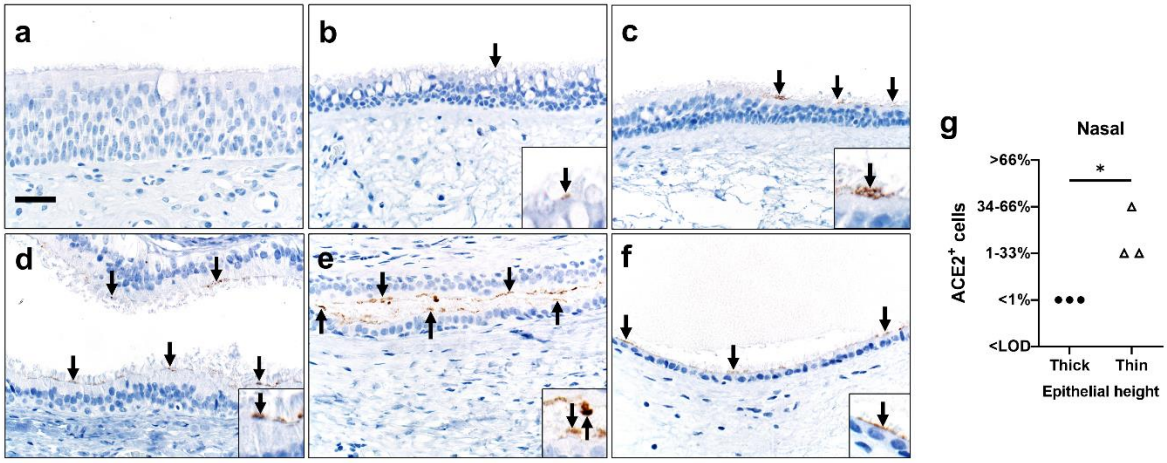

549

550 **Figure 5.** Detection of ACE2 protein (brown color, arrows and insets, **a-f**) and tissue scoring (**g**)
551 in representative sections of nasal tissues. **a, b**) In thick pseudostratified epithelium (PSE) ACE2
552 protein was absent (**a**) to rare (**b**) and apically located on ciliated cells. **c**) Tissue section shows a
553 transition zone from thick (left side, > ~4 nuclei) to thin (right side, ≤ ~4 nuclei) PSE and ACE2
554 protein was restricted to the apical surface of the thin PSE. **d-f**) ACE2 protein was detected
555 multifocally on the apical surface of ciliated cells in varying types of thin PSE, even to simple
556 cuboidal epithelium (**f**). Bar = 30 μm. **g**) ACE2 protein detection scores for each subject were
557 higher in thin than thick epithelium, (P=0.05, Mann-Whitney U test). LOD: Limit of detection.

558

559 **Supplemental information:**

Supplemental Figure 1

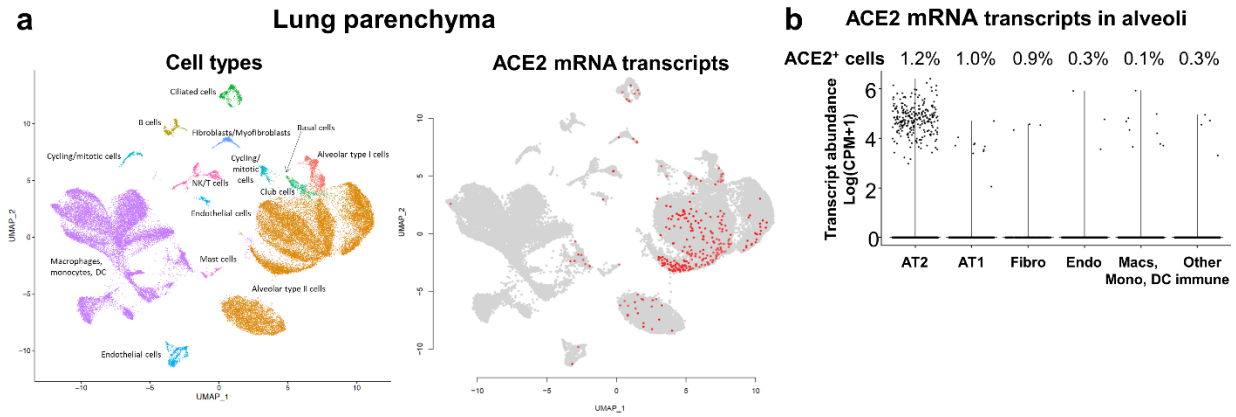

560

561 **Supplemental Figure 1.** Single-cell RNA sequencing reanalyses of ACE2 transcript abundance
562 in lung parenchyma (23). Summative observations from all donors. **a**) Uniform manifold
563 approximation and projection (UMAP) visualizations. Cells were clustered using a shared
564 nearest neighbor (SNN) approach. Cell types associated with each cluster were identified by
565 determining marker genes for each cluster. Each data point denotes a cell. On the right panel,
566 cells with ACE2 transcripts are shown in red. **b**) Violin plots representing ACE2 expression in
567 the alveoli. Airway cells (basal, mitotic, ciliated, club) are not shown. Percentage of $ACE2^+$ cells
568 within each cell type shows ACE2 transcripts in 1.2% of alveolar type II cells and in 0.1% of
569 macrophages, monocytes, or dendritic cells. Each data point denotes a cell, most cells have no
570 expression (0). AT2: alveolar type II. AT1: alveolar type I. Macs: Macrophages. Mono:
571 Monocytes. DC: dendritic cells. Other immune cells: B cells, mast cells, natural killer/T cells.
572 Endo: Endothelial. Fibro: Fibroblasts/myofibroblasts. NK: Natural killer. CPM: Counts per
573 million.

574

Supplemental Figure 2

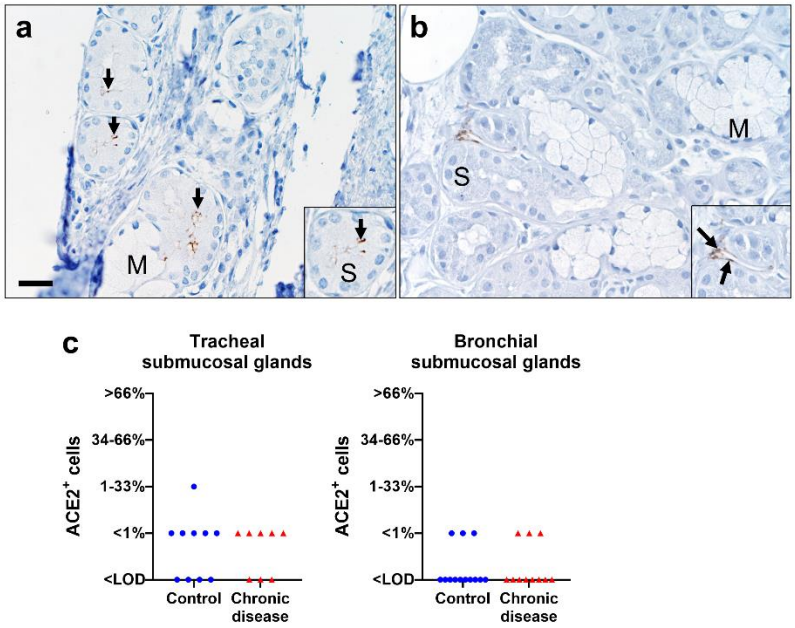

Supplemental Figure 2. Representative tissue section from submucosa of large airways (trachea/bronchi) showing ACE2 protein localization (brown color, black arrows) (**a, b**) and scores (**c**). **a**) Submucosal glands had uncommon to localized apical ACE2 protein (arrows) in serous (S) cells, but not mucous (M) cells. **b**) Submucosal glands also had absent to uncommon ACE2 protein (arrows) in the interstitium that centered on vascular walls and endothelium. This vascular staining was uncommonly seen in lung too and corresponded to the low levels seen in transcripts for these endothelial cells (Supplemental Figure 1a-b). Note the absence of ACE2 staining in serous (S) or mucous (M) cells of the gland (**b**). **c**) ACE2 protein scores for each subject for serous cells in submucosal glands from trachea and bronchi, in control versus chronic disease groups (P>0.9999, 0.9999, respectively, Mann-Whitney U test). Bar = 25 μm. LOD: Limit of detection.

Supplemental Figure 3

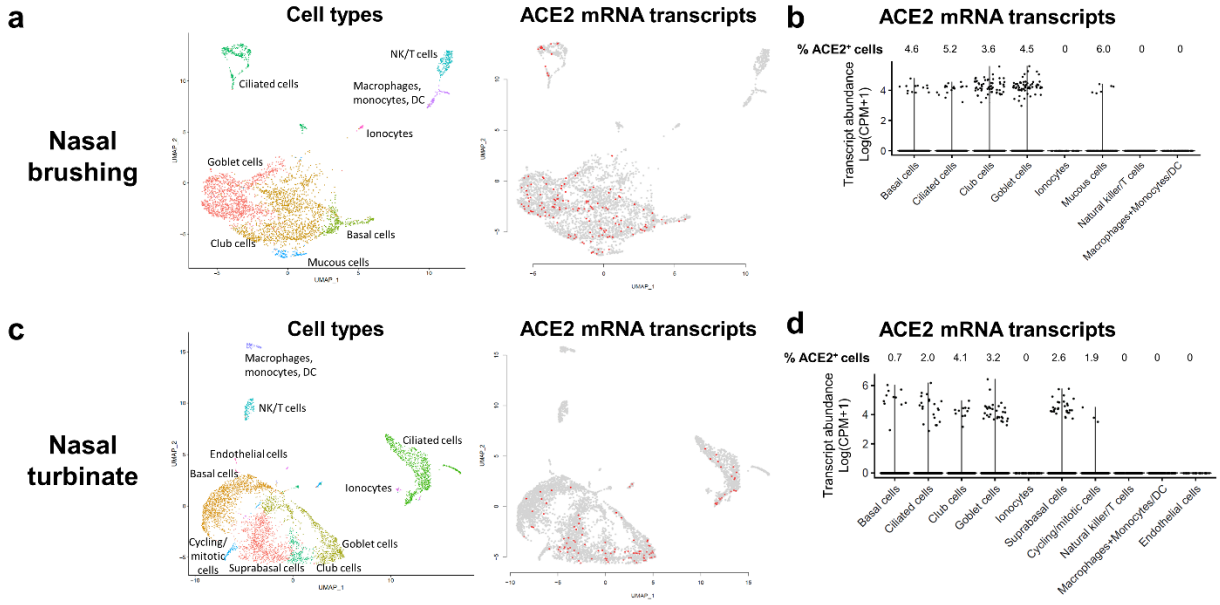

Supplemental Figure 3. Single-cell RNA sequencing reanalyses of ACE2 transcript abundance in nasal brushing (**a, b**) and nasal turbinate (**c, d**) (24). **a, c**) Uniform manifold approximation and projection (UMAP) visualizations. Cells were clustered using a shared nearest neighbor (SNN) approach. Cell types associated with each cluster were identified by determining marker genes for each cluster. Each data point denotes a cell. On the right panels, cells with ACE2 transcripts are shown in red. **b, d**) Violin plots representing ACE2 expression. In nasal turbinate and nasal brushing, percentage of $ACE2^+$ cells within each cell type shows ACE2 expression on epithelial cells. Each data point denotes a cell, most cells have no expression (0). DC: dendritic cells. NK: Natural killer. CPM: Counts per million.

Supplemental Figure 4

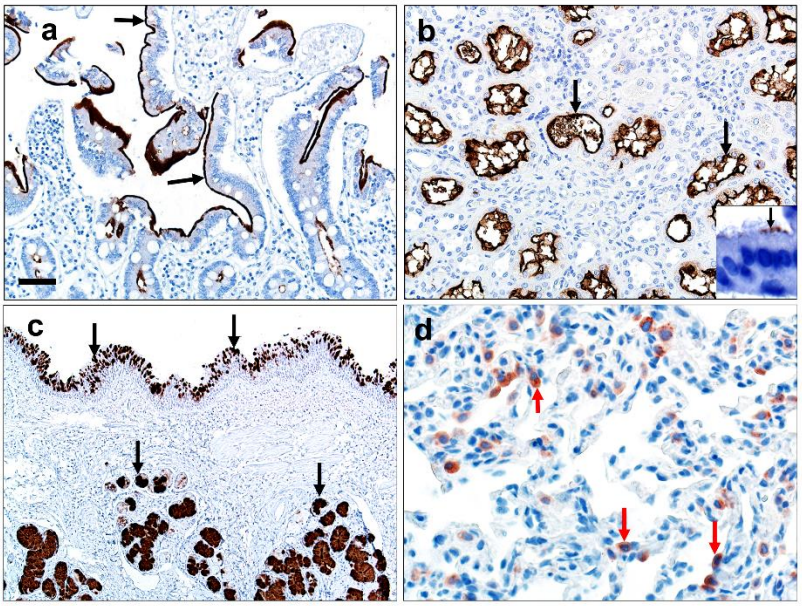

Supplemental Figure 4. Quality controls for ACE2 immunohistochemistry technique (**a, b**) and tissue quality (**c, d**). **a, b**) ACE2 protein (brown color, black arrows) was detected along the apical surface of small intestine enterocytes (**a**), renal tubule epithelium (**b**), and ciliated cells (**b, inset**) of primary airway cell cultures. These findings demonstrate specific detection of ACE2 protein in cells/tissues consistent with known ACE2 expression. **c**) Representative immunostaining of bronchus detected abundant MUC5B protein (brown color, black arrows) in mucous cells of surface epithelium (top) and submucosal glands (bottom). **d**) Representative sections of alveoli had SP-C$^+$ alveolar type II cells (red color, red arrows). These results (**c, d**) demonstrate the tissues were intact and that immunostaining can be used to detect native airway (**c**) and lung (**d**) proteins. Bar = 40 (a, b), 80 (c), and 20 μm (d).

Supplemental Figure 5

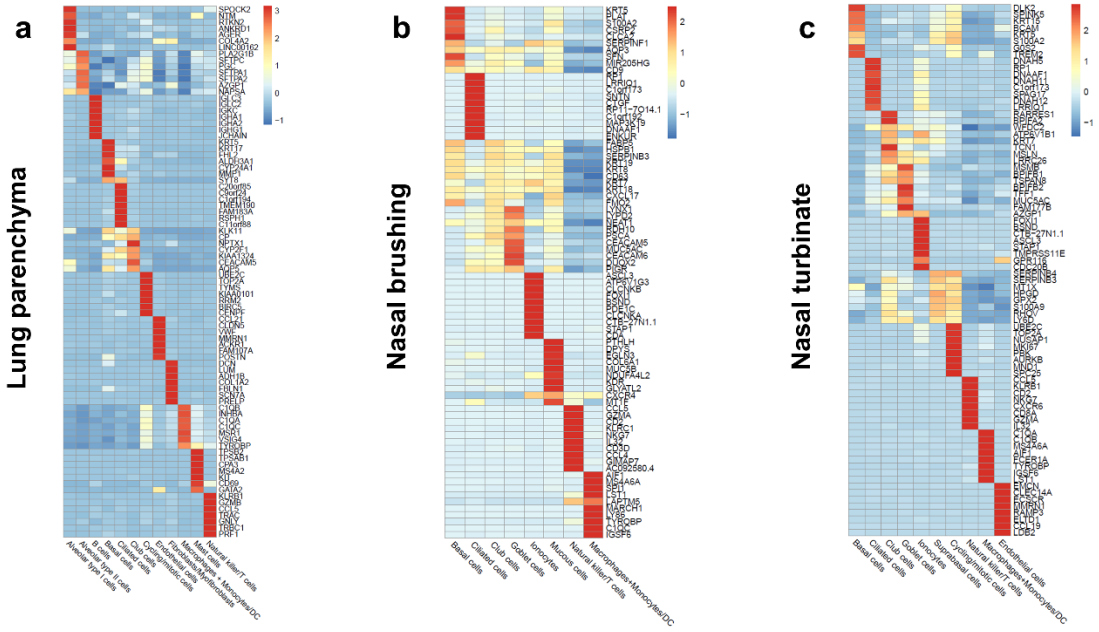

Supplemental Figure 5. Single-cell RNA sequencing reanalyses of lung parenchyma (a) (23), nasal brushing (**b**) and nasal turbinate (**c**) (24). Heatmaps depicting the marker genes for each cluster that were used to assign cell types.

615 **Supplemental Table 1. ACE2 protein reported in surface epithelium (SE) of human**

616 **respiratory tract surface epithelium.**

Reported Cases [n]	Primary Ab	SN	T	B	Br	Al	Summary comments
Non-diseased lungs / nasal [5 each]; diseased lungs [5] (17)	Polyclonal	SE (C++, basal cells in squamous epithelium)	n.d.	SE (C+)	n.d.	AT1 (C++); AT2 (C++)	Abundant ACE2 protein in lung epithelia
Non-diseased lungs [5] (18)	Undefined	n.d.	SE (C+, A+)	SE (C+, A+)	n.d.	"Alveoli" (A+) Mac (A+)	ACE2 is present on epithelia in several parts of the respiratory tract and macrophages
Lung [undefined] (19)	Polyclonal	n.d.	n.d.	SE (C+, N+, M+)	n.d.	AT1− AT2 (N+)	ACE2 is present in bronchial epithelium, AT2 cells and macrophages
Sinus [undefined] and Lung [undefined, same tissues as above] (20)	Polyclonal	SE (N++)	SE (−)	SE (C+, N++)	n.d.	AT1− AT2 (N++)	ACE2 is present in sinus and bronchial epithelium, AT2 cells and macrophages

617

618 Non-diseased: The cause of death was not directly related to lung disease

619 n.d.: Not described

620 Tissues: Sinonasal (SN), trachea (T), bronchi (B), bronchioles (Br), and alveoli (Al)

621 Cellular localization: cytoplasmic (C), nuclear (N), apical membrane (A)

622 Cells: Surface epithelium (SE), alveolar type I cells (AT1), alveolar type II cells (AT2), alveolar

623 macrophages (Mac)

624 ACE2 protein (based on published reports/figures): negative (−), weak (+), moderate to abundant

625 (++)

626 **Supplemental Table 2. Donor demographics and ACE2 distribution scores for each tissue**

627 **region.**

Case #	Group	Age (yrs)	Sex	Comorbidities	Trachea	Bronchi	Bronchioles	Alveoli
1	Control	5	F	Trauma	NA	2	2	1
2	Control	57	M	Arrhythmia	0	0	0	1
3	Control	31	M	Stroke (Joubert syndrome)	1	1	0	0
4	Control	53	F	Trauma	NA	0	0	1
5	Control	2	M	Brain hemorrhage	0	0	0	1
6	Control	2	M	Trauma	0	0	1	2
7	Control	0.5	M	Spinomuscular atrophy	NA	0	1	0
8	Control	71	M	Stroke, Parkinson's disease, nonsmoker	0	1	1	0
9	Control	4	F	Trauma	0	0	0	2
10	Control	1.2	M	Trauma	0	NA	1	1
11	Control	53	F	Trauma, nonsmoker	0	0	2	0
12	Control	26	F	NA	0	NA	0	0
13	Control	27	F	NA	NA	0	1	0
14	Control	64	M	NA	NA	1	1	0
15	Chronic disease	53	F	Smoker	0	NA	0	1
16	Chronic disease	60	M	COPD, smoker	NA	NA	0	1
17	Chronic disease	32	M	COPD, smoker	0	0	0	1
18	Chronic disease	68	M	COPD	NA	1	0	1
19	Chronic disease	68	F	COPD	NA	NA	1	1
20	Chronic disease	9	M	Asthma	0	0	0	1
21	Chronic disease	25	F	Cystic fibrosis	NA	0	0	0
22	Chronic disease	47	F	Cardiovascular disease	1	2	2	1
23	Chronic disease	27	M	Cystic fibrosis	0	NA	NA	1
24	Chronic disease	50	F	Cardiovascular disease, diabetes, asthma	NA	0	0	0
25	Chronic disease	37	M	Drug use, smoker	0	0	0	0
26	Chronic disease	38	M	Asthma (status asthmaticus)	0	0	0	0
27	Chronic disease	32	M	Cystic fibrosis	NA	NA	0	1
28	Chronic disease	58	F	Cardiovascular disease, diabetes, NASH	0	0	0	1
29	Chronic disease	19	F	Cystic fibrosis	NA	0	0	0

628

629 NA: Not available for analyses / COPD: Chronic obstructive pulmonary disease / NASH: Non-

630 alcoholic steatohepatitis.

631 Scoring: 0 = below limit of immunohistochemical detection; 1 = rare (<1%); 2 = 1-33%; 3 = 34-

632 66%; 4 = >66% of cells.

633

Supplemental Table 3. Parameters for immunohistochemistry on fixed tissues.

Target	Primary Antibody	Antigen Retrieval	Secondary Reagents
Allograft Inflammatory Factor 1 (AIF1)	Anti-AIF1 polyclonal (#019-19741, Wako Pure Chemical Industries, Ltd., Richmond, VA USA) in diluent 1:1000 x 1 hour	HIER, Citrate buffer pH 6.0, 110˚C for 15 min; 20 min cool down (Decloaking Chamber Plus, Biocare Medical, Concord, CA USA)	Dako EnVision+ System-HRP Labeled Polymer Anti-rabbit, 30 min (Dako North America, Inc., Carpentaria, CA USA) AEC chromogen, counterstain.
Angiotensin-Converting Enzyme 2 (ACE2)	Anti-ACE2, monoclonal (MAB933, R&D Systems, Minneapolis, MN USA) in diluent at 1:100 x 1 hour.	HIER, Citrate Buffer, pH 6.0, 110˚C for 15 minutes; 20 min cool down (Decloaking Chamber Plus, Biocare Medical, Concord, CA USA)	Dako EnVision+ System-HRP Labeled Polymer Anti-mouse, 60 min (Dako North America, Inc., Carpentaria, CA USA), DAB Chromogen, counterstain.
MUC5B	Rabbit anti-MUC5B polyclonal, (LSBio #LS-B8121, LifeSpan BioSciences, Inc., Seattle, WA) in Dako Antibody Diluent (Dako North America, Inc., Carpentaria, CA); 1:60,0000/30 min	HIER, Citrate buffer pH 6.0, 110˚C for 15min; 20 min cool down	Step 1: Biotinylated anti-Rabbit IgG (H+L) (Vector Laboratories, Inc., Burlingame, CA) in Dako Wash Buffer (Dako North America, Inc., Carpentaria, CA); 1:500, 30 min Step 2: Vectastain ABC Kit (Vector Laboratories, Inc., Burlingame, CA), 30min. DAB Chromogen, counterstain.
Surfactant Protein – C (SP-C)	Anti-SP-C, polyclonal (PA5-71680, Thermo Fisher Scientific, Waltham, MA USA) in diluent 1:100 x 1 hour	HIER, Citrate Buffer, pH 6.0, 110˚C for 15 minutes; 20 min cool down (Decloaking Chamber Plus, Biocare Medical, Concord, CA USA)	Dako EnVision+ System-HRP Labeled Polymer Anti-rabbit, 60 min (Dako North America, Inc., Carpentaria, CA USA), AEC chromogen, counterstain.

HIER – Heat-induced epitope retrieval

DAB – 3,3'-Diaminobenzidine (produces brown stain)

AEC - aminoethyl carbazole (produces red stain)

Counterstain – Harris hematoxylin (blue color)